

Unified RF-SVM model based digital radiography classification for Inferior Alveolar Nerve Injury (IANI) identification.

Manikandaprabhu P*, Karthikeyan T

PSG College of Arts and Science, India.

Abstract

This paper proposes a feature selection based classification method that can be applied to better accuracy in the Digital Radiographs (DR) for the identification of Inferior Alveolar Nerve Injury (IANI). Different conventional features based on the shape and EZW (Embedded Zero tree Wavelet) based texture features are extracted using different feature extraction techniques. Then, aggregate voting of all the decision trees in the Random Forest (RF) method to get the reduced feature. Finally, Support vector machine (SVM) with RBF kernel is trained using reduced features to classify the IAN (Inferior Alveolar Nerve) injured on a healthy object. The proposed classification results are compared with PCA-DT, PCA-MLP and PSO-MLP classification algorithms. Both training and testing stages of proposed model get better classification accuracy of 96.4% and 83.58% respectively. This shows the highest classification accuracy performance among some other existing methods.

Keywords: Digital radiographs, Feature selection, Inferior alveolar nerve injury, Random forest, Support vector machine.

Accepted on March 30, 2016

Introduction

Medical demands have driven the fast growth of medical image processing methods, which in turn have significantly promoted the level of the therapeutic process. They have become essential tools for diagnosis, treatment planning and authentication of administered treatment. Therefore, the technology of medical image processing has long attracted attention of relevant experts. Nowadays, panoramic radiography is regularly used in dental practice, because it provides visualness of anatomical structures in pathological changes of the teeth, jaws and temporo-mandibular joints.

A dental implant is surgically inserted into the jawbone as an artificial root onto which a dental prosthesis is placed. Inferior Alveolar Nerve injury (IANI) is the main problematical significance of dental surgical procedures and has major medico-legal implications [1]. These injuries results in fractional or absolute loss of consciousness from the ipsilateral skin of the lower lip and cheek, the buccal oral mucosa in this area and the lower teeth. Causes of IANI include placement of dental implants, local anesthetic injections, third molar surgery, endodontic, trauma and orthognathic surgery.

IANI and Lingual Nerve (LN) injuries are considered to be suitable to mechanical irritations from surgical interference and are inclined by numerous demographic, anatomic and treatment-related factors [2]. Most patients who extend an IANI gradually get back to regular consciousness above the path of a few weeks or months, depending upon the nerve

damage severity. Nevertheless, after the most rigorous injuries, where fraction/fracture or all of the nerves have been sectioned and the place may have been compromised by infection, revival will be imperfect. Therefore, identification of the IAN is essential when using preoperative planning software for dental implant surgery.

The IAC has a hollow tubular shape but is difficult to detect because its structure is not well defined and because it is frequently connected to nearby hollow spaces. Hence, accurate and automatic identification of the IAN canal is a challenging issue. The IAC is outlined by two thin radiopaque outlines to signify the cortical walls of the canal. IAC appears lower or superimposed above the apex of the mandibular molar teeth [4]. Thus, the majority of earlier researches on the IAC detection [5] require users' intervention such as a manual trace of the IAN canal. Damage to the IAN can yield very serious complications [3].

On panoramic Digital Radiography (DR) observation, the root apex of the mandibular second molar was in close propinquity to the mandibular canal while the apices of the mesial and distal roots of the mandibular first molar were the farthest from the canal [6]. Radiological prediction of injury to the IAN depends on the relationship of the root to the canal discussed by Malik [7]. Rood and Shebab [8] has defined seven vital

recommendations that can be taken from OPG images. There have been several OPG assessment researches which maintain the effectiveness of these seven findings [9]. It must be renowned, even if, that the statistical results from these analysis had various levels of specificity and sensitivity in Table 1. Nowadays, research decided that high-risk signs were known by OPG in particular; darkening of the root is closely related to cortical bone loss and/or grooving of the root [9].

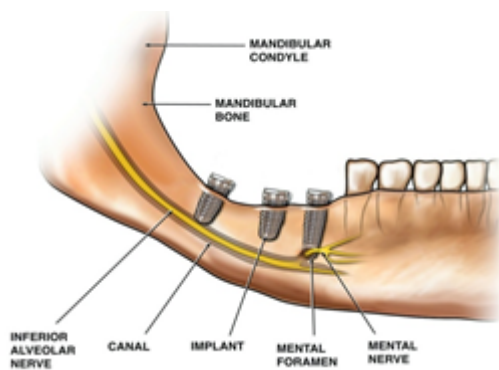


Figure 1. Anatomy of IAN.

OPG Imaging procedure	Sensitivity (%)	Specificity (%)
Darkening of the root	32-71	73-96
Interruption of the canal	22-80	47-97
Diversion of the canal	3-50	82-100

Table 1. Specificity and sensitivity for predicting IAN injury with third molar surgery in OPG image [9].

Image classification [10] automatically assigns an unknown image to a category according to its visual content, which has been a major research direction in computer vision. Feature

extraction step affects all other subsequent processes. Visual features were categorized into primitive features such as colour, shape and texture. However, as X-ray images are gray level images and do not contain any colour information, the related image analysis systems mostly deal with textures for feature extraction process which were used by several researchers [11–14]. A multi-visual feature mixture such as GLCM, shape based canny edge detector feature and pixel value was presented by Mueen et al. [15]. Other authors have also combined pixel value as a global image descriptor with other image representation techniques to construct feature vector of the image [16].

Texture analysis has a major role for medical image analysis. Gray level co-occurrence matrices (GLCM) [17] are commonly used feature extraction techniques in the above works. GLCM histogram has extracted the feature vector used for Digital Radiograph (DR) analysis by Yu et al. [11]. Texture based geometric pattern feature analysis method to analyze the DR developed by Katsuragawa et al. [12]. GLCM and embedded zero tree wavelet features are extracted using PCA-DT classification method in [13]. PCA-MLP classification method has proposed in [14] using embedded zero tree wavelet and GLCM features. Here, Random Forest [RF] is used as feature selection method [18]. From a classification point of view, support vector machine (SVM) is a popular method for binary classification. Zhu et al. [19] proposed SVM with Gaussian kernel classifier evaluate the benign and malignant pulmonary modules. Yuan et al. [20] assess the breast cancer prognosis classification using SVM with better accuracy than other classifiers. It automatically identifies the medical related messages using SVM model outperformed [21]. Therefore, in this work SVM is used as a classification tool.

Proposed Methodology

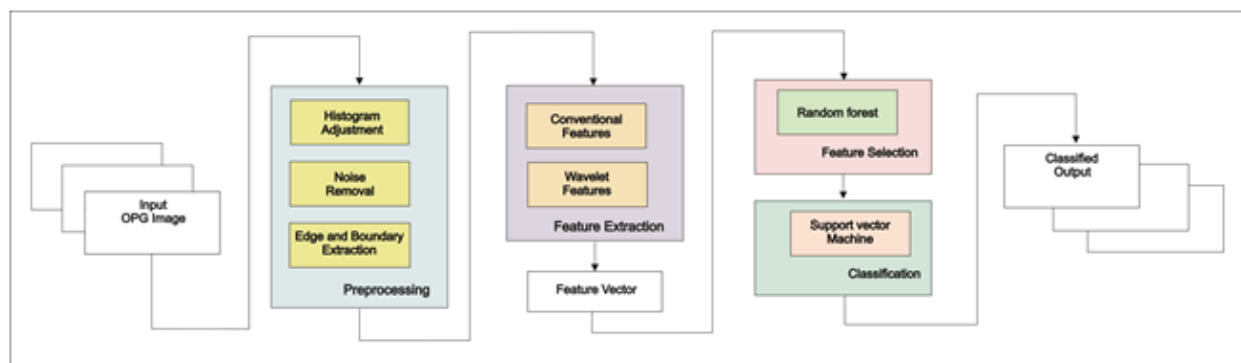


Figure 2. Proposed Methodology.

Proposed Methodology framework shown in Figure 2 is as follows:

- Preprocessing
- Feature Extraction
- Feature Selection
- Classification

Preprocessing

Preprocessing consists of normalizing the intensity variations, low contrast, removing low frequency noise, removing reflections and masking segment of images. This step is a major role in the perfect and precise extraction of features.

Histogram adjustment, noise removal and canny based edge extraction are sublevel of this process.

Histogram adjustment: It is used to emphasize and highlight the details of input images and to justify their gray level histogram [22]. In this case, the contrast of all images is increased by mapping the values of the input intensity image of new values such that, 1% of the data is saturated at low and high intensities of the input data (Figure 3).

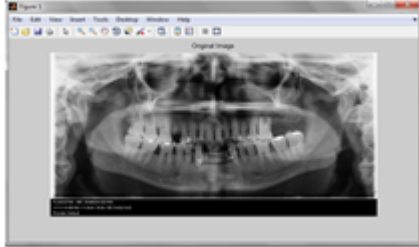


Figure 3. OPG image before preprocessing.

Noise removal: To get rid of noise and unnecessary information, the anisotropic diffusion filter as proposed in [23] is utilized. This filter removes the noise from input image while preserves important parts of image contents such as edges and major boundaries. The filtered image is modeled as the solution to the anisotropic diffusion equation as follows:

$$\frac{\partial u(x, y, t)}{\partial t} = \text{div}(g(|\nabla u(x, y, t)|) \nabla u(x, y, t)) \quad (1)$$

where $u(x, y, t): \Omega \times [0, +\infty] \rightarrow R$ is a scale image and $g(|\nabla u|)$ is a decreasing function depending on the gradient of u .

Edge and boundary extraction: An edge gives us an object layout. Identifying the pixel value and it is compared with the neighboring pixels to be outlined as edge regions [24]. All objects in the image are outlined when the intensities are measured exactly [25]. In order to extract the edges and boundaries from images, canny edge detection algorithms [24] is utilized. In Canny edge detection procedure for segmentation shows in Figure 4.

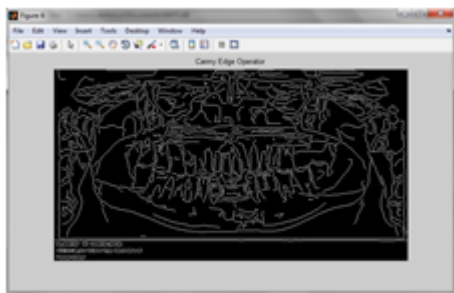


Figure 4. OPG image for After Edge and Boundary Detection.

Feature extraction

Mostly, image classification use low level features color, shape and texture. But, DR images are mainly in grey level. So, color is not suitable feature for DR analysis. Then, shape and texture can be considered for DR analysis [12]. Here, we extracted the conventional features in Figure 5 as follows: Shape, Region

properties, Tamura features, entropy and Wavelet based Texture Features for two-Dimensional level discrete wavelet transform for four (LL, LH, HL and HH) sub-bands in θ directions ($\theta=0^\circ, 45^\circ, 90^\circ, 135^\circ$). Here, there are 383 features are extracted from each DR image.

Shape features: Shape provides geometrical information of an object in an image. This geometrical information is remained same even when the location, scale and orientation of the object are changed. In this study, the shape information of an image is described based on its edges. A histogram of the edge directions is used to represent shape attribute for each image and image patches.

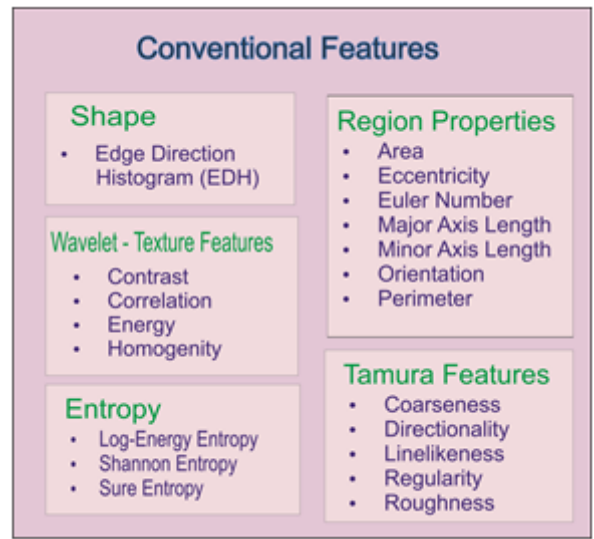


Figure 5. Conventional features.

Edge direction histogram (EDH): For each pixel p_{ij} , its edge vector is defined as $\vec{D}_{i,j} = \{dx_{i,j}, dy_{i,j}\}$, where $dx_{i,j}$ and $dy_{i,j}$ are obtained by the vertical edge mask and horizontal edge mask respectively. The edge vector can be also represented as its amplitude and direction, the amplitude can be roughly estimated by

$$\text{Amp}_{i,j} = |dx_{i,j}| + |dy_{i,j}| \quad (2)$$

The angle representing the pixel's edge direction is decided by

$$\text{Ang}_{i,j} = \frac{180^\circ}{\pi} \times \arctan\left(\frac{dy_{i,j}}{dx_{i,j}}\right) \quad (3)$$

Each pixel in the image has an edge vector containing its edge amplitude and direction, and all the pixels' edge vectors form the image's edge map. It must be noted that in the actual implementation of the algorithm, equation (3) is not necessary. In this paper, the $dx_{i,j}/dy_{i,j}$ is used to express the pixel's edge direction.

The edge direction histogram [26] is used to compare the edge information between the distorted image blocks and the reference ones. In this paper, the continual direction (0°~180°) is divided into 8 discrete directions which are shown in Figure 6 and are not the same as reference [26].

For each image block, its edge direction histogram can be obtained by the following steps:

Step 1. Calculate each pixel's edge amplitude and direction by equations (2) and (3) respectively.

Step 2. Quantify each pixel's direction as one of the 8 discrete directions (see Figure 6).

Step 3. Sum up all the pixels' edge amplitudes with the same direction in the block.

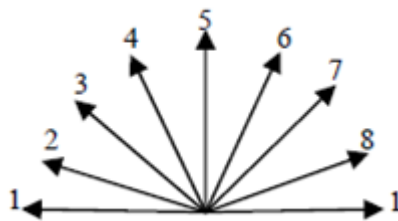


Figure 6. The 8 discrete directions.

Now edge direction histogram (vector) is obtained. An example of a 16 × 16 image block and its edge direction histogram are showed in Figure 7.

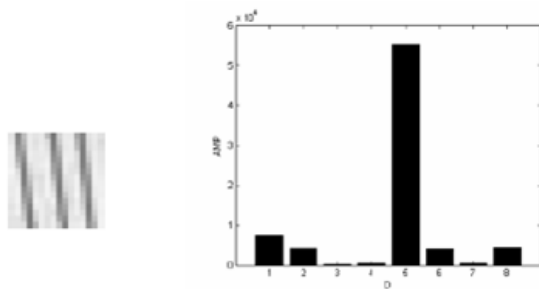


Figure 7. A 16 × 16 image block and its edge direction histogram, D represents the directions and AMP represents the amplitude.

Wavelet-texture features: Various statistical features are derived from the segmented image for classification [17]. But it is a challenging task to extract a good feature set for classification. GLCM features are based on the joint probability distribution of matchup of pixels. Distanced and angle θ within a given neighborhood are used for computation of joint probability distribution between pixels. Normally $d=1, 2$ and $\theta=0^\circ, 45^\circ, 90^\circ, 135^\circ$ are used for computation [27]. Hence, 32 features totally obtained each DR image. In our proposed system the following GLCM features are extracted [28]:

Energy (k1) which expresses the repetition of pixel pairs of an image,

$$k1 = \sum_{i=0}^{N-1} \sum_{j=0}^{k-1} p_{\mu}^2(i, j) \tag{4}$$

Local variations (k2) which present in the image is calculated by Contrast. If the contract value is high, the image has large variations.

$$k2 = \sum_{t=0}^{N-1} t^2 \left\{ \sum_{i=0}^{N-1} \sum_{j=0}^{k-1} p_{\mu}^2(i, j) \right\} \tag{5}$$

Correlation (k3) is a measure linear dependency of grey level values in co-occurrence matrices. It is a two dimensional frequency histogram in which individual pixel pairs are assigned to each other on the basis of a specific, predefined displacement vector.

$$k3 = \sum_{i=0}^{k-1} \sum_{j=0}^{k-1} \frac{(i, j)p(i, j) - \mu_1\mu_2}{\sigma_1^2\sigma_2^2} \tag{6}$$

Homogeneity (k4) is inversely proportional to contrast at constant energy whereas it is inversely proportional to energy.

$$k4 = \sum_{i=0}^{k-1} \sum_{j=0}^{k-1} \frac{p_{\mu}(i, j)}{1 + (i - j)^2}, i \neq j \tag{7}$$

Wavelet transform can capture both frequency and spatial information and has merits of multi-resolution and multi-scale decomposition [29,30]. The selection of the wavelet base is very important in practical applications of DWT. When analyzing the same problem, a different wavelet basis will produce a different result. So far, there has been no good way or a unified standard to solve the problem, and the main method used is to determine a wavelet base that is applicable for a problem according to the error between the results derived from wavelet analysis and the theoretical results.

In our study, we selected the well-known Zero tree Wavelet as the wavelet base, which may provide a more effective analysis than others in the scenario of image processing. In order to perform the DWT, the image has to be a square image, and its row/column size must be an integer power of 2. So, technically, the EZW is applicable to the square images of sizes in integer powers of 2 (for example, image sizes like 128 x 128 or 512 x 512). This transformation is theoretically lossless, although this may not always be the case. The purpose of the transformation is to generate decorrelated coefficients, which means it removes all the dependencies between samples.

The EZW algorithm applies Successive Approximation Quantization in order to provide multi-precision representation of the transformed coefficients and to facilitate the embedded coding. The algorithm codes the transformed coefficients in decreasing order in several scans. Each scan of the algorithm consists of two passes: significant map encoding and refinement pass. The dominant pass scans the subband structure in zigzag, right-to-left and then top-to-bottom within each scale, before proceeding to the next higher scale of subband structure as presented in Figure 8.

Feature Selection Methods	Number of Features Selected
Before Feature Selection	383
PCA	41
PSO	45
RF	35

Table 2. Summary of Feature Selection.

Classification

In mid-1990s, Vapnik [38] introduced Support Vector Machine (SVM). It performs well in small sample sizes and in high dimensional spaces [19]. It also exploits the least feasible quadratic programming issues, which determines systematically and promptly. It improves the scaling and computing time significantly. It executes the lowest sequential maximization procedure to train a classifier using linear kernels.

Support Vector Machine (SVM) is a kernel based technique that represents one of the major developments in machine learning algorithm. SVM is a group of supervised learning methods that can be applied for classification and regression. It learns by example to assign labels to objects. SVM has shown its capacities in pattern recognition and a better performance in many domains compared with other machine learning techniques. SVMs have also been successfully applied to an increasingly wide variety of biological applications. Based on empirical results and several classification applications in automatic classification of medical X-ray images, SVM has shown a better generalization performance compared with other classification techniques [40-42].

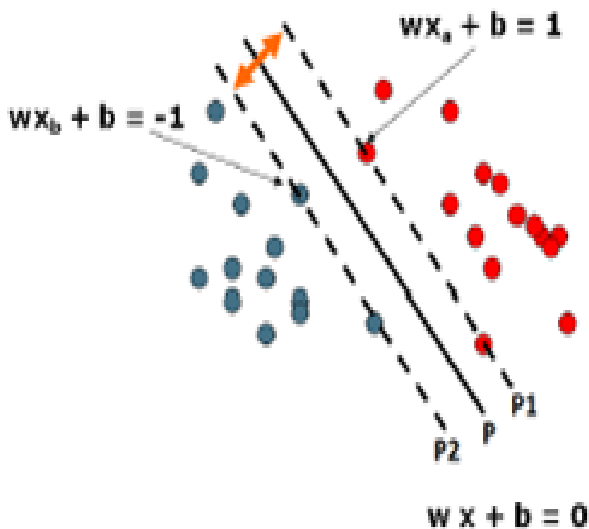


Figure 9. The basics of classification by SVM.

SVM algorithm takes a set of input data points. It then decides that the data point belong to which possible two classes. The aim is to construct a hyperplane or set of hyperplanes in a high or infinite dimensional space that classifies the data more accurately. Therefore, the basic idea is to find a hyperplane that has the greatest distance to the nearest training data points of any class.

A hyperplane can be defined by the following equation:

$$wx + b = 0 \quad (10)$$

Where x is the data point lying in the hyperplane, w is normal vector to hyperplane and b is the bias. Figure 9 and 10 show the basics of SVM.

The idea is to separate two classes (red circle and blue circle), each are labeled as 1 and -1 respectively. Those circles which lie on p1 and p2 are support vectors. For all data points from the hyperplane p ($wx + b = 0$), the distance between origin and the hyperplane p is $(|b|/||w||)$. We consider the patterns from the class -1 that satisfy the equality $wx + b = -1$, and determine the hyperplane p1; the distance between origin and the hyperplane p1 is equal to $|-1-b|/||w||$.

Similarly, the patterns from the class +1 satisfy the equality $wx + b = +1$, and determine the hyperplane p2; the distance between origin and the hyperplane p2 is equal to $|+1-b|/||w||$. Of course, hyperplanes P, P1, and P2 are parallel and no training patterns are located between hyperplanes P1 and P2. Based on the above considerations, the margin between hyperplanes P1 and P2 is $2/||w||$.

In order to use the SVM methodology to handle the classes are not linearly separable, then the input vectors such as low level feature vectors are mapped to higher dimensional feature space H via a nonlinear transformation, $R^d \rightarrow H$. The kernel function ($K(x_i, x_j)$) is used then to construct optimal hyperplane in this high dimensional feature space. This kernel function is a products of input vector x_i and x_j where $K(x_i, x_j) = \Phi(x_i) \cdot \Phi(x_j)$. Radial Basis Function (RBF) kernel and Polynomials kernel are the most common mappings:

Polynomials kernel: $K(x_i, x_j) = (x_i \cdot x_j + 1)^q$. (q is the degree of Polynomial)

Radial Basis Function (RBF) kernel: $K(x_i, x_j) = e^{-||x_i - x_j||^2 / 2\sigma^2}$ (σ is the Gaussian sigma)

The above description of SVM is designed for binary classification which only deals with two class labels +1 and -1. It can be extended to multi-class classification where each data point x can be mapped to a specific label y from the set of available labels.

In our proposed system the classification has two divisions: i) training stage and ii) testing stage. In the training stage, various features are extracted from the IAN identified and not identified images. In testing stage based on the knowledge base, the classifier classifies the image into IAN- identified and not identified images. Figure 10 shows the Proposed RF-SVM model for feature selection based classification model.

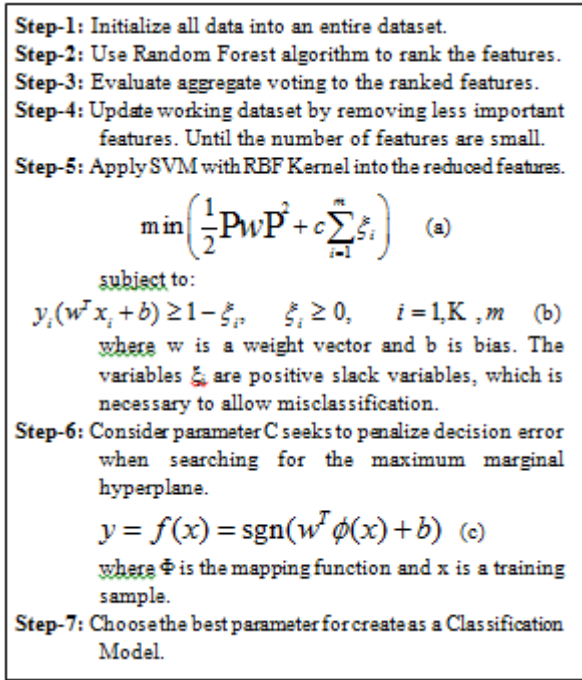


Figure 10. Proposed Model for RF-SVM.

Experimental Results and Discussions

Data description

Here, 140 OPG DRs collected from MSR Tooth Clinic, Madurai which is composed of 62 OPG radiographs for male patients of age of 10 to 75 years old and 38 for female patients of age of 12 to 74 years old. Around 40 OPG radiographs are posterior dental implants for accuracy of implant position and injuries of IAN. The diagnostic decisions of all the 100 patients were made by a radiologist panel. Table 3 show the summary of experimental data of OPG image and Patients Data Summary with Sex and Age Range in Table 4.

Table 3. Summary of Experimental Data.

Patient (Years)	Age	Sex	Number of Patients	Number of DRs	Data Dimensions
10-75		Male-62 Female-38	100	140	1024 × 564 × 24

Table 4. Patients Data Summary with Sex and Age Range.

Age Range	Male	Female	Total
10 to 20	15	8	23
21 to 35	27	20	47
36 to 50	22	17	39
51 to 65	10	8	18
66 to 75	9	4	13

Total	83	57	140
-------	----	----	-----

Performance assessment

In this study, classification accuracy, sensitivity and specification were used as assessment of the proposed RF-SVM model. It defined in Equation (11), (12) and (13).

$$Accuracy = \frac{TP + TN}{TP + FN + TN + FP} \times 100\% \quad (11)$$

$$Sensitivity = \frac{TP}{TP + FN} \times 100\% \quad (12)$$

$$Specificity = \frac{TN}{TN + FP} \times 100\% \quad (13)$$

where TP(True Positive) denote the number of correctly classified IAN injured object, TN(True Negative) denote the number of correctly classified healthy object, FP(False Positive) denote the number of normal cases incorrectly classified. IAN denotes injured object and FN (False Negative) denotes the number of irregular objects incorrectly classified as normal object.

Comparison of classification performance

The obtained experimental results from the proposed technique are given in Table 5 and Table 6. The accuracy of SVM classification accuracy is better than Decision Tree (DT) and Multilayer Perceptron (MLP) classifiers. Both training and testing stages of Random Forest (RF) - Support Vector Machine (SVM) get better classification accuracy of 96.4% and 83.58% respectively. The graphical result Figures 11 and 12 showed the comparison of proposed results with existing Results [13,14,39].

Table 5. Comparison of Training results with Different classifiers.

Feature Selection - Classifier	Classification Accuracy	Sensitivity	Specificity
PCA - DT [13]	82.3	76.2	85.2
PCA - MLP [14]	85.4	76.6	90.2
PSO - MLP [39]	88.7	85.2	88.5
RF - SVM (Proposed)	96.4	88.2	99.1

Table 6. Comparison of Testing results with Different classifiers.

Feature Selection - Classifier	Classification Accuracy	Sensitivity	Specificity
PCA - DT [13]	78.58	68.6	76.8
PCA - MLP [14]	79.29	69.9	83.8
PSO - MLP [39]	80.71	77.6	80.5
RF - SVM (Proposed)	83.58	79.9	92.8

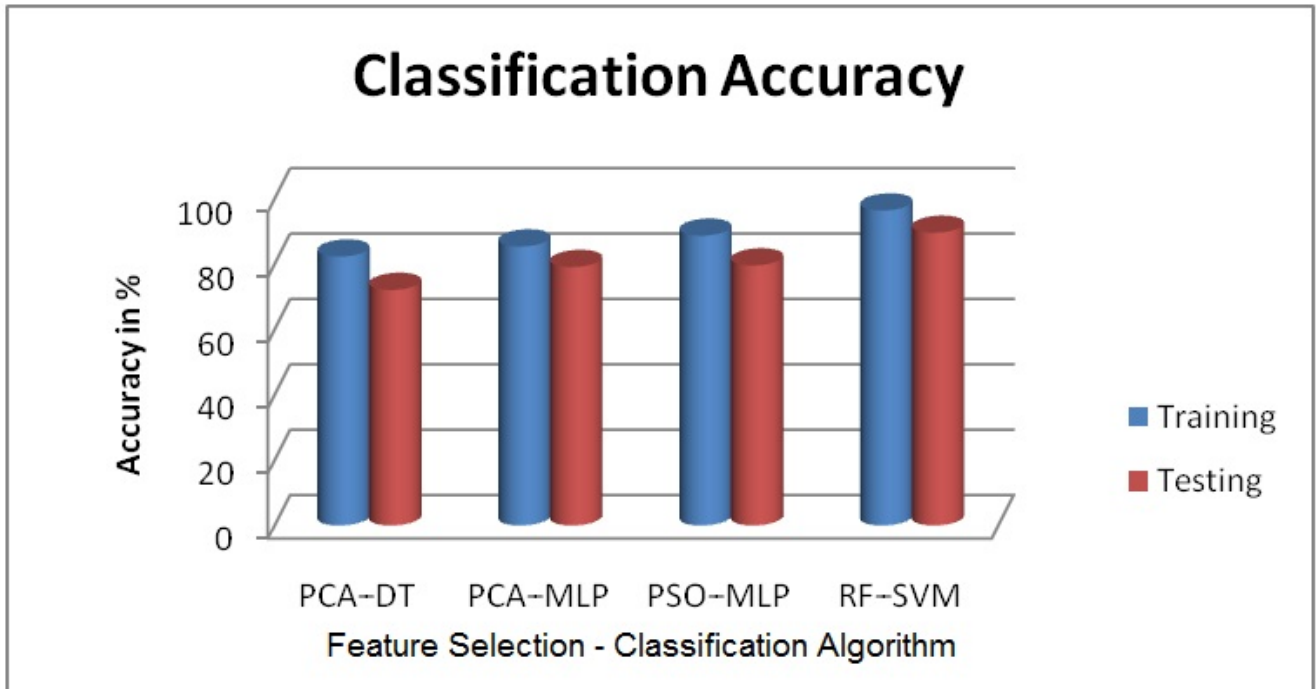


Figure 11. Performance analysis for classification accuracy.

Figure 12. Performance analysis for Sensitivity and Specificity for training and classification stage.

In the proposed system, experimental results are compared to medical expert results with proposed system results in Table 7.

Table 7. Comparison of Different Classifier Results with Medical Experts.

IAN Identification	Medical Experts			PCA-DT		PCA-MLP		PSO-MLP		RF-SVM	
	No. Images	of %		No. Images	of %	No. Images	of %	No. Images	of %	No. of Images	%
Not Identified	12	8.57		8	5.71	7	5	7	5	5	3.57
Partially Identified	25	17.86		22	15.71	22	15.71	20	14.29	18	12.86
Clearly identified	103	73.57		110	78.58	111	79.29	113	80.71	117	83.58

Above the experimental data in table 7, we got the following results.

Not identified in IAN from medical experts 8.57%, but the proposed system has 3.57% only.

Partially identified in IAN, 17.86% for medical experts and 12.86% for the proposed system.

Clearly identified in IAN, 73.57% for medical experts, 83.58% for proposed system.

The total number of partial and clearly identified IAN is 91.43% for medical experts and 96.44% for proposed system. Comparatively, the proposed system clearly identified IAN is 5% more than medical experts. So, the proposed system has improved accuracy of IAN identification then medical experts. Figure 13 shows the graphical representation of medical expert results with proposed system results.

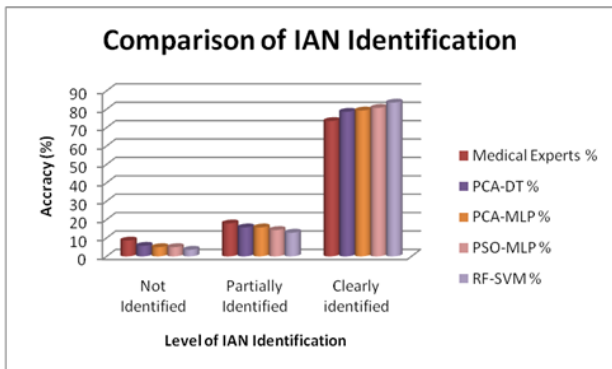


Figure 13. Comparison of IAN Identification.

In Tables 8-12 to be discussed in the age range classification of IAN identification with medical experts, PCA-DT, PCA-MLP, PSO-MLP and RF-SVM respectively. Below the age of 15 and more than age of 65, the visibility of IAN is very limited.

Table 8. Summary of IAN identification for medical experts.

Age Range	Not Identified		Partially Identified		Clearly identified	
	Male	Female	Male	Female	Male	Female
10 to 20	4	2	7	5	4	1
21 to 35	0	0	2	1	25	19
36 to 50	0	0	1	0	21	17
51 to 65	1	0	1	2	8	6
66 to 75	3	2	5	1	1	1
Total	8	4	16	9	59	44

Table 9. Summary of IAN Identification for PCA-DT Classifier.

Age Range	Not Identified		Partially Identified		Clearly identified	
	Male	Female	Male	Female	Male	Female
10 to 20	3	1	6	5	6	2
21 to 35	0	0	2	0	25	20
36 to 50	0	0	1	0	21	17
51 to 65	0	0	1	1	9	7

66 to 75	2	2	5	1	2	1
Total	5	3	15	7	63	47

Table 10. Summary of IAN Identification for PCA-MLP Classifier.

Age Range	Not Identified		Partially Identified		Clearly identified	
	Male	Female	Male	Female	Male	Female
10 to 20	2	1	6	4	7	3
21 to 35	0	0	0	1	27	19
36 to 50	0	0	1	0	21	17
51 to 65	0	0	1	2	9	6
66 to 75	2	2	5	2	1	1
Total	4	3	13	9	65	46

Table 11. Summary of IAN Identification for PSO-MLP Classifier.

Age Range	Not Identified		Partially Identified		Clearly identified	
	Male	Female	Male	Female	Male	Female
10 to 20	2	1	5	4	8	3
21 to 35	0	0	1	0	26	20
36 to 50	0	0	1	0	21	17
51 to 65	0	0	1	1	9	7
66 to 75	3	1	6	1	1	1
Total	5	2	14	6	65	48

Table 12. Summary of IAN Identification for RF-SVM Classifier.

Age Range	Not Identified		Partially Identified		Clearly identified	
	Male	Female	Male	Female	Male	Female
10 to 20	2	1	10	3	3	4
21 to 35	0	0	0	0	27	20
36 to 50	0	0	0	0	22	17
51 to 65	0	0	1	0	9	8
66 to 75	1	1	2	2	6	1
Total	3	2	13	5	67	50

Conclusion

In this paper, unified RF-SVM model based on EZW based texture and shape features are proposed. It was performed on a database consisting 140 DRs. By the aim of improving the classification accuracy, different conventional features are extracted. Then, Random Forest based Support Vector Machine model was used for feature selection and classification process. Experimental results shows that our method is an effective feature selection method obtain higher classification accuracy of other methods. Other performance analysis like sensitivity and specificity of our proposed model perform get better than

other methods. The provided results show effectively classifies the IANI identification.

References

- Mischkowski RA, Zinser MJ, Neugebauer J, Kubler AC, Zoller JE. Comparison of static and dynamic computer-assisted guidance methods in implantology. *Int J Computerized Dentistry* 2006; 9: 23-35.
- Mansoor J. Pre-and postoperative management techniques. Before and after. Part 1: medical morbidities. *British dental journal* 2015; 218; 273-278.
- Modi CK, Desai NP. A simple and novel algorithm for automatic selection of ROI for dental radiograph segmentation. in *Proc. 24th IEEE CCECE* 2011; 504-507.
- Haring JI, Jansen L. *Dental radiography: principles and techniques*. London: W. B. Saunders Company 2000; 342-362.
- White SC, Pharoah MJ. *Oral radiology: principles and interpretation*. Elsevier Health Sciences 2014.
- Iwao S, Ryuji U, Taisuke K, Takashi Y. Rare courses of the mandibular canal in the molar regions of the human mandible: A cadaveric study. *Okajimas folia anatomica Japonica* 2014; 82: 95-102.
- Malik NA. *Textbook of Oral and Maxillofacial Surgery*. 2nd ed, New Delhi: Jaypee Brothers Medical Publishers 2008.
- Kim HG, Lee JH. Analysis and evaluation of relative positions of mandibular third molar and mandibular canal impacts. *Journal of the Korean Association of Oral MaxillofacSurg* 2014; 40: 278-284.
- Kim JW, Cha IH, Kim SJ, Kim MR. Which risk factors are associated with neurosensory deficits of inferior alveolar nerve after mandibular third molar extraction. *J Oral MaxillofacSurg* 2012; 70: 2508-2514.
- Karthikeyan T, Manikandaprabhu P. Analyzing Urban Area Land Coverage Using Image Classification Algorithms. *Computational Intelligence in Data Mining-Volume 2, Smart Innovation, Systems and Technologies, Springer India* 2015; 32: 439-447.
- Yu P, Xu H, Zhu Y, Yang C, Sun X, Zhao J. An automatic computer-aided detection scheme for pneumoconiosis on digital chest radiographs. *J Digit Imaging* 2011; 24: 382-393.
- Katsuragawa S, Doi K, MacMahon H, Monnier-Cholley , Morishita J, Ishida T. Quantitative analysis of geometric-pattern features of interstitial infiltrates in digital chest radiographs: preliminary results. *J Digit Imaging* 1996; 9: 137-144.
- Karthikeyan T, Manikandaprabhu P. A Novel Approach for Inferior Alveolar Nerve (IAN) Injury Identification using Panoramic Radiographic Image. *Biomed Pharma Jour* 2015; 8: 307-314.
- Karthikeyan T, Manikandaprabhu P. A Study on Digital Radiographic Image Classification for Inferior Alveolar Nerve Injury(IAN) Identification using Embedded Zero Tree Wavelet. *International Journal of Applied Engineering Research* 2015; 10: 599-604.
- Mueen A, Zainuddin R, Sapiyan Baba M. Automatic Multilevel Medical Image Annotation and retrieval. *J Digit Imaging* 2008; 21: 290-295.
- Tommasi T, Orabona F, Caputo B. Discriminative cue integration for medical image annotation. *Pattern Recogn Lett* 2008; 29: 1996-2002.
- Haralick RM, Shanmugam K, Dinstein I. Textural features for image classification. *IEEE Trans Syst Man Cybern* 1973; 3: 610-621.
- Han L, Embrechts M, Szymanski B, Sternickel K, Ross A. Random forests feature selection with K-PLS: detecting ischemia from magnetocardiograms. in *Proc. ESANN, Bruges, Belgium* 2006; 221-226.
- Zhu Y, Tan Y, Hua Y, Wang MP, Zhang G, Zhang JG. Feature selection and performance evaluation of support vector machine (SVM)-based classifier for differentiation benign and malignant pulmonary nodules by computed tomography. *J Digit Imaging* 2010; 23: 51-65.
- Yuan QF. *Cancer Diagnosis by Using Support Vector Machine*. MD dissertation, Chongqing University 2007.
- Lu Y. Automatic topic identification of health-related messages in online health community using text classification *Springer plus* 2013; 309.
- Ghofrani F, Helfroush M, Danyali H, Karimi K. Medical X-ray image classification using gabor-based CS local binary patterns. in *Proc. ICEBEA* 2012.
- Fu S, Ruan Q, Wang W, Li Y. Adaptive anisotropic diffusion for ultrasonic image denoising and edge enhancement. *Int J Info Tech* 2006; 2: 284-292.
- Canny J. A computational approach to edge detection. *IEEE Trans Pat Anal Mach. Intell* 1986; 8: 679-698.
- Jian M, Liu L, Guo F. Texture image classification using perceptual texture features and Gabor wavelet features. in *Proc APCIP* 2009.
- Feng P, Xiao L, Rahardja S. Fast mode decision algorithm for intraprediction in H.264/AVC video coding. *IEEE Trans. Circuits and Syst. Video Tech* 2005; 813- 822.
- Gelzinisa A, Verikasa A, Bacauskienea M. Increasing the discrimination power of the co-occurrence matrix-based features. *Pattern Recogn* 2004; 40: 2367-2372.
- Subramoniam M, Barani S, Rajini V. A non-invasive computer aided diagnosis of osteoarthritis from digital x-ray images. *Biomedical Research* 2015; 26: 721-729.
- Arivazhagan S, Ganesan L. Texture segmentation using wavelet transform. *Pattern Recogn Lett* 2003; 24: 3197-3203.
- Kociólek M, Materka A, Strzelecki M, Szczypiński P. Discrete Wavelet Transform –Derived Features for Digital Image Texture Analysis”. in *Proc. Int. Conf. Signals and Electronic Systems*. Lodz, Poland: IEEE 2001.
- Wu PC, Chen LG. An efficient architecture for two-dimensional discrete wavelet transform. *IEEE Trans. Circuits and Syst Video Tech* 2001; 11: 536-545.

32. Masood K, Rajpoot N. Spatial analysis for colon biopsy classification from hyperspectral imagery. *Annals of the BMVA* 2008; 2008: 1-6.
33. Muller H, Cramer JK, Eggel I, Bedrick S, Reisetter J, Kahn CE Jr, Hersh W. Overview of the CLEF 2010 medical image retrieval track. in *Proc CLEF 2010 Workshop* 2010.
34. Prasad BG, Krishna AN. Performance evaluation of statistical textural features for medical image classification. in *Proc National Conference on Emerging Trends in Computer Science* 2011.
35. Coifman RR, Wickerhauser MV. Entropy-based algorithms for best basis selection. *IEEE Trans Information Theory* 1992; 38: 713-718.
36. Vasantha M, Bharathi DVS, Dhamodharan R. Medical image feature, extraction, selection and classification. *Int J Engg Sci & Tech* 2010; 2: 2071-2076.
37. Breiman L. Random forests. *Machine Learning* 2001; 45: 5-32.
38. Vapnik VN, Vapnik V. *Statistical Learning Theory*. Newyork: Wiley 1998.
39. Karthikeyan T, Manikandaprabhu P. Feature Selection Based Hybrid Classification Algorithm with Embedded Zero Tree Wavelet. *ARNP J Engg Appl Sci* 2015; 10: 1723-1731.
40. Mueen A, Zainuddin R, Sapiyan Baba M. Automatic multilevel medical image annotation and retrieval. *J Digit Imaging* 2008; 21: 290-295.
41. Rahman MM, Desai BC, Bhattacharya P. Medical image retrieval with probabilistic multi-class support vector machine classifiers and adaptive similarity fusion. *Comput Med Imaging Graph* 2007; 32: 95-108.
42. Unay D, Soldea O, Ozogur-Akyuz S, Cetin M, Ercil A. Medical image retrieval and automatic annotation: VPA-SABANCI at ImageCLEF 2009. in *Proc Cross-Language Evaluation Forum (CLEF) Workshop in conjunction with ECDL'09 Corfu Greece* 2009.

***Correspondence to:**

Manikandaprabhu P

Department of Computer Science,

PSG College of Arts & Science,

Coimbatore,

Tamilnadu, India